

PRO-Face S: Privacy-preserving Reversible Obfuscation of Face Images via Secure Flow

Lin Yuan, Kai Liang, Xiao Pu, Yan Zhang, Jiaxu Leng, Tao Wu, *Member, IEEE*, Nannan Wang, *Member, IEEE*, and Xinbo Gao, *Senior Member, IEEE*

Abstract—This paper proposes a novel paradigm for facial privacy protection that unifies multiple characteristics including anonymity, diversity, reversibility and security within a single lightweight framework. We name it PRO-Face S, short for Privacy-preserving Reversible Obfuscation of Face images via Secure flow-based model. In the framework, an Invertible Neural Network (INN) is utilized to process the input image along with its pre-obfuscated form, and generate the privacy protected image that visually approximates to the pre-obfuscated one, thus ensuring privacy. The pre-obfuscation applied can be in diversified form with different strengths and styles specified by users. Along protection, a secret key is injected into the network such that the original image can only be recovered from the protection image via the same model given the correct key provided. Two modes of image recovery are devised to deal with malicious recovery attempts in different scenarios. Finally, extensive experiments conducted on three public image datasets demonstrate the superiority of the proposed framework over multiple state-of-the-art approaches.

Index Terms—facial privacy protection, image obfuscation, invertible neural network.

I. INTRODUCTION

ADVANCEMENTS of video capturing and analytic technologies have brought tremendous convenience to public, but on the negative side, have also raised growing concerns over privacy. Personal face photos being captured and published (intentionally or unintentionally) are prone to being abused by unauthorized parties, exposing great threats to individuals privacy and security. The case of ClearView AI [1] collecting personal photos and training facial recognition systems without users consent raised the alert on hidden privacy

This work is supported by the National Natural Science Foundation of China under Grant No. 62201107, 62036007 and U22A2096, in part by the Natural Science Foundation of Chongqing under Grand No. CSTB2022NSCQ-MSX1265 and CSTB2022NSCQ-MSX1342, in part by the Chongqing Excellent Scientist Project under Grant No. cstc2021ycjh-bgzxm0339, and in part by the Creative Research Groups of Chongqing Municipal Education Commission under Grant CXQT21020. (*Corresponding author: Xinbo Gao.*)

Lin Yuan, Xiao Pu, and Tao Wu are with the School of Cyber Security and Information Law, Chongqing University of Posts and Telecommunications, Chongqing 400065, China (e-mail: yuanlin@cqupt.edu.cn; puxiao@cqupt.edu.cn; wutao@cqupt.edu.cn)

Kai Liang and Nannan Wang are with the School of Optoelectronic Engineering, Chongqing University of Posts and Telecommunications, Chongqing 400065, China; Nannan Wang is also with the School of Telecommunications Engineering, Xidian University, Xi'an 710071, China (e-mail: kailiang777@qq.com; nnwang@xidian.edu.cn)

Yan Zhang, Jiaxu Leng and Xinbo Gao are with the School of Computer Science and Technology, Chongqing University of Posts and Telecommunications, Chongqing 400065, China (e-mail: yanzhang1991@cqupt.edu.cn; lengjx@cqupt.edu.cn; gaobx@cqupt.edu.cn)

threats behind public face images. Breach of surveillance cameras [2] implies tremendous privacy and security risks underneath video surveillance systems, especially when not being properly regulated or secured. China's first lawsuit on facial recognition [3] initiated by Professor Guo in Hangzhou also drew public attention towards the legality and privacy of ubiquitous face recognition systems.

In academia, facial privacy protection methodologies (aka anonymization, de-identification, or DeID) have been extensively studied to deal with the privacy threats induced by either unauthorized machine recognition or unexpected human inspection. Early approaches utilize traditional image processing techniques to distort facial appearance in image, such as filtering [4], masking [5], various transformation [6]. With advancements of deep learning especially various generative models, diversified methods have been proposed to anonymize the facial appearance in image such that the the protected face looks differently from the original. Different groups of solutions feature distinctive characteristics and advantages. Conventional approaches are widely used in practice due to its simplicity and strong obfuscation effect to human, but are considered to be less effective in protecting privacy against machine vision. Generative approaches offer novel measures to hide the identity information while preserving the natural facial appearance. Although seemingly promising, this type of approaches are still barely applied in practice due to ongoing arguments and potential legal issues related to generative fake media. *Hence, we are motivated to design a unified methodology that can assemble multiple obfuscations into one to provide users with full flexibility in choosing the desired one for fitting different applications.*

In this paper, we stand on a fresh view and propose a novel paradigm for facial privacy protection that unifies multiple excellent characteristics at once. We name it **PRO-Face S**, short for **Privacy-preserving Reversible Obfuscation of Face** images via a **Secure flow-based** model. In such a framework (as illustrated in Fig. 1), the input image to be protected is first pre-obfuscated by a privacy-preserving image operation. Then, both the original and the pre-obfuscated images are fed into an invertible flow-based network, generating the protection image that visually approximates the pre-obfuscated one. Relying on the intrinsic network invertibility, the original image can be recovered with high fidelity using the same set of model parameters as protection, in need of visual inspection or forensics. Specially, the protection network is conditioned on

arXiv:2307.09146v1 [cs.CV] 18 Jul 2023

a user-specified secret such that the correct recovery can only be achieved when the correct secret is available. While, any malicious recovery attempt using a wrong secret key will only produce distorted or obfuscated recovery images.

Therefore, our framework elegantly unites multiple merits an ideal visual privacy protection method should have:

- **Diversity:** Unlike existing approaches where “diversity” usually indicates diverse facial identities corresponding to different secret keys, we redefine the term to a broader notion indicating diverse types of visual obfuscations to support wider use cases.
- **Anonymity:** Due to the diversity in visual obfuscations to be applied, the framework offers different degrees of personalized anonymity depending on the type and strength of user-specific obfuscation.
- **Reversibility:** Thanks to the intrinsic invertibility of the flow-based model, the framework can easily achieve high quality image recovery with reduced number of model parameters, less training efforts, and better interpretability.
- **Security:** Relying on a specially designed keying mechanism, the protection and recovery processes are mutually controlled by a secret key, which ensures correct recovery only when the correct secret key is available.
- **Lightweight:** Last but not least, the framework encapsulates a limited number of invertible blocks with less than 1M parameters to achieve optimal protection and recovery performances, which make it applicable for more practical applications.

This paper makes the following contributions:

- 1) A novel *one-size-fits-all* paradigm for facial privacy protection is proposed, which integrates multiple merits including diversity, anonymity, reversibility and security into a single lightweight framework.
- 2) A novel key-based mechanism controlling forward (protection) and backward (recovery) passes of flow-based model is devised, which ensures secure image protection and high quality recovery simultaneously.
- 3) Extensive experiments and comprehensive analysis on privacy, reversibility and security of the proposed framework are presented. In addition, a small set of pre-processed 3K images is provided as a standard benchmark for fair comparison in future research of the area.

II. RELATED WORK

This section reviews the literatures that are most relevant to ours, and points out our inspirations from existing studies.

A. Image Processing Approaches

Early research towards facial privacy protection mainly uses conventional image processing to conceal sensitive information (such as face) from input images [7]. Proposed approaches can be roughly categorized into masking-based methods [5], filtering-based methods [4], [8], and transformation-based methods [6], [9]. Different methods offer different degrees and styles of visual obfuscation. Although considered to offer less utility and limited reversibility, this group of approaches are still popularly used in practice, due to their simplicity and strong obfuscation effect.

B. Deep-based Facial Anonymization

The success of deep learning technologies has greatly boosted the research of face privacy protection towards diversified directions. A group of adversarial-based approaches [10]–[13] have proven their success in fighting against unauthorized face recognition. However, they do not mean to protect image privacy against human inspection. Another group of approaches utilize generative models to create natural facial appearance different from original. Early studies in this group include head inpainting [14], DeepPrivacy [15], live face de-identification [16], and CIAGAN [17]. Recent efforts have been devoted to more sophisticated solutions covering multiple utility properties such as diversity, reversibility, security, and identifiability. Gu et al. [18] first proposes reversible face identity transformer that performs face anonymization and de-anonymization upon a binary password. Cao et al. [19] proposes a personalized invertible DeID framework where protection and recovery are implemented by transforming disentangled ID vector with user-specified password. Wu et al. [20] designs PECAM, which performs privacy-enhanced securely-reversible video transformation in video streaming and analytics systems. Li et al. [21], [22] proposes identity-preserved facial anonymization via identity-aware region discovery to determine facial attributes sensitive to human eyes. Hugo et al. [23] proposes UU-Net, a reversible face DeID framework powered by two U-Nets for protection and recovery respectively, to be in a photorealistic and seamless way in video surveillance. Yuan et al. [24] devises an Identifiable Virtual Face Generator (IVFG) to produce the virtual faces that are recognizable via their virtual ID embeddings. Wen et al. [25] attempts to protect facial privacy in video frames via a modular architecture named IdentityMask, which leverages deep motion flow and protective motion IdentityMask, Zhang et al. [26] proposes RAPP, a reversible privacy-preserving scheme for protecting various facial attributes. Recently, Li et al. [27] proposes RiDDLE, a reversible DeID framework with StyleGAN [28] latent space encryption.

C. Template-based Face Anonymization

A small group of research utilizes a template-based methodology to generate the anonymized face that approximates a pre-obfuscated template. You et al. [29] proposes a reversible privacy-preserving recognition framework that hides original image into its pixelated form, which can be later recovered based on a different network. Yuan et al. [30] introduces PRO-Face, which not only supports diverse facial obfuscations, but also preserves identity information in the protected faces. However, PRO-Face does not take into account reversibility by design. Recently, Yang et al. [31] first utilizes invertible neural network (INN) to build an invertible mask network (IMN) to achieve the state-of-the-art protection and recovery performance in the category of research. However, no security property has been considered in the IMN framework. The design of our method is highly inspired by PRO-Face [30] and IMN [31], whereas multiple usable features are integrated into one framework with optimal performance achieved on each aspect.

D. Invertible Neural Networks

Invertible neural network (INN) is a special network structure that employs a flow of bijective mapping functions to perform invertible transformation between inputs and outputs. The inputs to the INN model can be easily recovered from the outputs using the same model parameters by inverting the bijective transformations. INN was first proposed by Dinh et al. [32] as Non-linear Independent Components Estimation (NICE) to model complex probability densities. It was later adapted to handle image processing tasks by Dinh et al. [33] using convolutional coupling layers. Later, Kingma et al. [34] proposes Glow, a generative flow with invertible 1×1 convolutions, for more efficient and realistic image generation. Due to the excellent performance, INN has been used in many image-related tasks including image-to-image translation [35], [36], image scaling [37], super-resolution [38], denoising [39], compression [40], steganography [41], [42], and face anonymization [31].

Specifically, our study is greatly inspired by HiNet [41] and DeepMIH [42], two invertible image steganography frameworks with excellent concealment and recovery performance. Similar as PRO-Face [30] and IMN [31], we also simulate the privacy protection process as image steganography, where the original private information is concealed into a pre-obfuscated template, which can be later recovered in case of need. Built on the similar INN structure of [42], we make elaborate security enforcement via a newly designed keying mechanism to ensure secure privacy protection and recovery. Moreover, we greatly reduce model parameters to make it more applicable to practical usages without sacrificing much performance.

III. PROBLEM FORMULATION

We first formulate the proposed privacy protection paradigm (illustrated in Fig. 1), consisting of three major steps: pre-obfuscation, key-based protection, and secure recovery.

A. Pre-Obfuscation

Given an input image $\mathbf{x} \in \mathbb{R}^{3 \times W \times H}$, it is first processed by an existing image obfuscator $\mathcal{O} : \mathbb{R}^{3 \times W \times H} \mapsto \mathbb{R}^{3 \times W \times H}$, resulting in the pre-obfuscated image $\mathbf{y} \in \mathbb{R}^{3 \times W \times H}$ that is significantly different from its original in terms of visual perception (noted by \mathcal{V}):

$$\mathbf{y} = \mathcal{O}(\mathbf{x}), \mathcal{V}(\mathbf{y}) \not\cong \mathcal{V}(\mathbf{x}). \quad (1)$$

The pre-obfuscated image is assumed to have visual privacy removed. Notably, the operation \mathcal{O} can be in principle any type of facial obfuscator in diversified and personalized form. Thus, the pre-obfuscator in the framework offers high diversity in terms of obfuscation effect, areas and strengths.

B. Key-based Protection

As the second step, both the original and the pre-obfuscated image (\mathbf{x}, \mathbf{y}) are fed into an invertible protection module \mathcal{P} , producing the protection image $\hat{\mathbf{y}} \in \mathbb{R}^{3 \times W \times H}$ that is visually

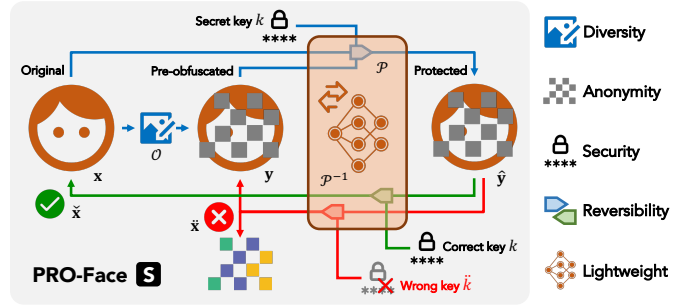


Fig. 1. Illustration of the PRO-Face S paradigm for facial privacy protection.

approximate to the pre-obfuscated one with high fidelity, and therefore being privacy-preserved:

$$\hat{\mathbf{y}} = \mathcal{P}(\mathbf{x}, \mathbf{y}, k), \mathcal{V}(\hat{\mathbf{y}}) \cong \mathcal{V}(\mathbf{y}). \quad (2)$$

Herein, a user-specified secret key k is injected into the protection network to condition the generation of the protection image. The role of the secret key is to control the mutual processes of protection and recovery such that the original face can only be recovered with the correct secret key.

C. Secure Recovery

It is possible to recover the original image from the protection image with high fidelity given the correct secret key k provided, by inverting the protection network (noted \mathcal{P}^{-1}) relying on the same model parameters:

$$\tilde{\mathbf{x}} = \mathcal{P}^{-1}(\hat{\mathbf{y}}, k), \mathcal{V}(\tilde{\mathbf{x}}) \cong \mathcal{V}(\mathbf{x}). \quad (3)$$

Using any wrong secret key \tilde{k} with even one bit difference from the original key, a wrong recovery image $\tilde{\mathbf{x}}$ will be resulted, which is significantly different from the original and fails to reveal any private visual information:

$$\tilde{\mathbf{x}} = \mathcal{P}^{-1}(\hat{\mathbf{y}}, \tilde{k}), \mathcal{V}(\tilde{\mathbf{x}}) \not\cong \mathcal{V}(\mathbf{x}) \quad (4)$$

Such a key-controlled image recovery process features the security of our framework.

Interestingly, the protection and recovery processes roughly simulate a cycle of symmetric cryptography, whereas the protection image in our case (corresponding to the ciphertext) still preserves meaningful semantics instead of being completely randomized as cryptography.

IV. THE FRAMEWORK DESIGN

The workflow of the PRO-Face S framework is illustrated in Figure 2, the core of which is an invertible protection network composed of a flow of Secure Affine Coupling Blocks (SACBs). We adopt the basic design of the affine coupling block (ACB) structure from [42], and make innovative security enforcement on it by integrating randomness into each ACB conditioned on secret keys. In addition, Discrete Wavelet Transform (DWT) and Inverse Wavelet Transform (IWT) modules are also employed following [42] to process input and output data, to better fuse the original image into the obfuscated template in the frequency domain, and to reduce

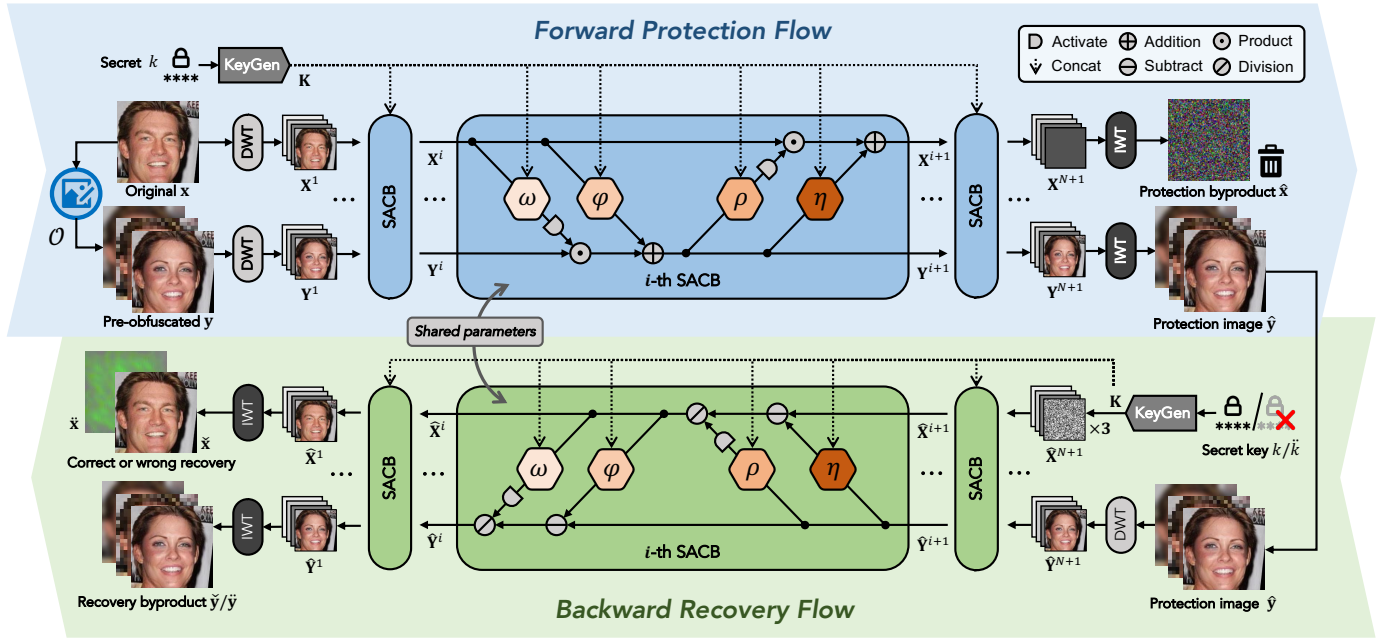


Fig. 2. The architecture of PRO-Face S composed of the forward protection and backward recovery flows featured by several core components: pre-obfuscation (\mathcal{O}), key generation (KeyGen), discrete wavelet transform and its inverse (DWT/IWT), and secure affine coupling block (SACB).

the computational cost. The distinctive design of our key generation module, and the image protection/recovery processes are described in detail as follows.

A. Secret Key Generation

The key generation module (KeyGen for short) aims to generate randomized information (named secret map) used to control the protection/recovery processes based on an user-specified secret input. Simulating cryptography, we expect any difference in bits of the input key would result in totally different output secret map. Illustrated by Fig. 3, the KeyGen module works as follows:

Given an initial key k with arbitrary characters and length (also known as password, to be specified by users), the Password-Based Key Derivation Function (PBKDF) is applied to derive from the initial key a binary code with fixed length of $W \times H$, which is then geometrically transformed into a 2D binary map \mathbf{k} with the same dimension as the input image (single channel):

$$\mathbf{k} = t(\text{PBKDF}(k)), \quad \mathbf{k} \in \{-1, 1\}^{W \times H}. \quad (5)$$

The binary map \mathbf{k} is further transformed into a four-channel secret map by DWT:

$$\mathbf{K} = \text{DWT}(\mathbf{k}), \quad (6)$$

where \mathbf{K} is in dimension of $(4 \times \frac{W}{2} \times \frac{H}{2})$. The secret map \mathbf{K} is the actual information integrated into the protection and recovery network for controlling the two processes mutually. Specifically, the version 2 of PBKDF (namely PBKDF2) with Hash-based Message Authentication Code (HMAC) pseudorandom function is applied, using a fixed salt and a small number of iterations (10 in our case) for demonstration purpose. The pseudorandomness of PBKDF2 ensures to output completely random secret map \mathbf{K} for any unique initial secret.

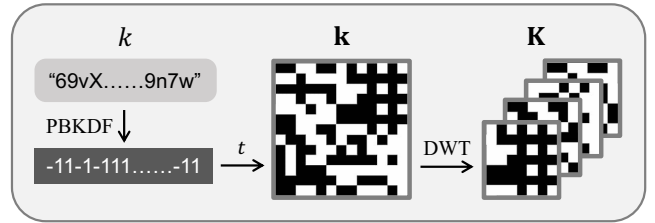


Fig. 3. Illustration of the KeyGen module: the initial secret k in arbitrary length is eventually mapped into a random secret map in shape $(4 \times \frac{W}{2} \times \frac{H}{2})$.

B. Forward Protection Flow

The forward flow of privacy protection is illustrated in the upper part of Fig. 2. In the protection pass, the input face \mathbf{x} is first obfuscated by an existing image obfuscator $\mathcal{O}()$, resulting in pre-obfuscated image $\mathbf{y} = \mathcal{O}(\mathbf{x})$. Then, both \mathbf{x} and \mathbf{y} are decomposed into wavelet sub-bands by DWT:

$$\mathbf{X}^1 = \text{DWT}(\mathbf{x}), \quad (7)$$

$$\mathbf{Y}^1 = \text{DWT}(\mathbf{y}). \quad (8)$$

which are further fed into N sequential Secure ACBs (SACBs for short).

Similar as [42], each SACB consists of four non-linear mapping functions noted $\omega()$, $\varphi()$, $\rho()$ and $\eta()$ respectively. Those functions share the same densely connected conv structure like DenseNet [43], without sharing parameters. A group of the four functions form a basic bijective ACB structure that is invertible. Uniquely, in our design, each of the function receives the fusion of the image feature maps and the secret map, achieved by concatenating the secret map \mathbf{K} into the image feature maps \mathbf{X}^i channel-wise without losing invertibility. That said, we replace $\omega(\mathbf{X}^i)$ in [42] with $\omega(\mathbf{X}^i \parallel \mathbf{K})$ etc. While, each

nonlinear function still outputs data in the same dimension as the input image feature map:

$$\omega, \varphi, \rho, \eta : \mathbb{R}^{(C+4) \times \frac{W}{2} \times \frac{H}{2}} \mapsto \mathbb{R}^{C \times \frac{W}{2} \times \frac{H}{2}}, \quad (9)$$

where $C = 3$ indicates the number of RGB image channels. The transformations of each SACB are formulated as:

$$\mathbf{Y}^{i+1} = \mathbf{Y}^i \cdot \exp(a(\omega(\mathbf{X}^i \parallel \mathbf{K}))) + \varphi(\mathbf{X}^i \parallel \mathbf{K}), \quad (10)$$

$$\mathbf{X}^{i+1} = \mathbf{X}^i \cdot \exp(a(\rho(\mathbf{Y}^{i+1} \parallel \mathbf{K}))) + \eta(\mathbf{Y}^{i+1} \parallel \mathbf{K}), \quad (11)$$

where \parallel indicates channel-wise concat and $i \in \{1, 2, \dots, N\}$. Specially, $a(\cdot)$ stands for Sigmoid multiplied by a constant factor, which acts as activation function to constrain the processed feature map. Being processed by N sequential SACBs, the wavelet sub-bands of the last block are transformed back to the spatial domain to produce two output images:

$$\hat{\mathbf{x}} = \text{IWT}(\mathbf{X}^{N+1}), \quad (12)$$

$$\hat{\mathbf{y}} = \text{IWT}(\mathbf{Y}^{N+1}), \quad (13)$$

where $\hat{\mathbf{y}}$ is designated as the final protection image that is visually identical to the pre-obfuscated image ensuring visual privacy. The other output $\hat{\mathbf{x}}$ is a sort of byproduct image which contains latent information lost during the protection process. Similar as [42], the byproduct $\hat{\mathbf{x}}$ is not required for recovery.

C. Backward Recovery Flow

In the recovery pass of [42], a noise image sampled from Gaussian distribution is used as auxiliary variable to replace the latent output lost in the forward pass. In our framework, since random secret information following uniform distribution is injected and input/protection images follow the same image distribution, we assume the protection byproduct $\hat{\mathbf{x}}$ also approximates the same case-agnostic distribution as the integrated secret map \mathbf{K} , although not necessarily the identical. Innovatively, we opt to apply the same secret key k in protection to substitute the lost latent output $\hat{\mathbf{x}}$ to perform image recovery. Therefore, the recovery process takes the protection image $\hat{\mathbf{y}}$ and the secret key k as inputs, and generates the recovery image highly similar to its original. Instead of sampling the secret key at random as [42], we enforce the image recovery work perform correctly only when the correct secret key is provided, while making the recovery towards a wrong direction distinct from the original image when any different secret key is applied.

Illustrated in the lower part of Fig. 2, the recovery process starts with transforming the protected image $\hat{\mathbf{y}}$ back into the wavelet domain $\hat{\mathbf{Y}}^{N+1} = \text{DWT}(\hat{\mathbf{y}})$ and generating the secret map using the same KeyGen module defined in Eq. (5) and (6) $\mathbf{K} = \text{KeyGen}(k)$. The secret map \mathbf{K} is repeated three times channel-wise to align with the dimension of the wavelet sub-bands of an RGB image $\hat{\mathbf{X}}^{N+1} = \mathbf{K} \parallel \mathbf{K} \parallel \mathbf{K}$, which is treated as the auxiliary input to the backward recovery process to substitute the discarded protection byproduct $\hat{\mathbf{x}}$. Then, both $\hat{\mathbf{X}}^{N+1}$ and $\hat{\mathbf{Y}}^{N+1}$ are processed by N backward SACBs via

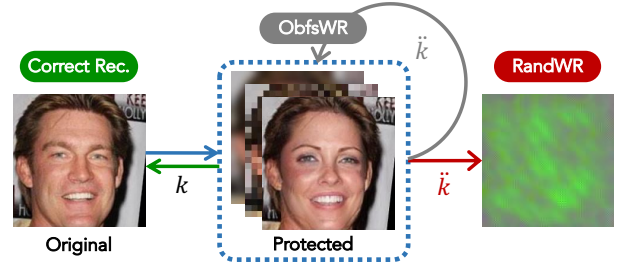


Fig. 4. Illustration of the two wrong recovery modes, RandWR and ObfsWR.

inverted bijective functions based on Eq. (10) and (11), with the secret map \mathbf{K} integrated in the same way as protection:

$$\hat{\mathbf{X}}^i = \left(\hat{\mathbf{X}}^{i+1} - \eta(\hat{\mathbf{Y}}^{i+1} \parallel \mathbf{K}) \right) \cdot \exp\left(-a\left(\rho\left(\hat{\mathbf{Y}}^{i+1} \parallel \mathbf{K}\right)\right)\right), \quad (14)$$

$$\hat{\mathbf{Y}}^i = \left(\hat{\mathbf{Y}}^{i+1} - \varphi(\hat{\mathbf{X}}^i \parallel \mathbf{K}) \right) \cdot \exp\left(-a\left(\omega\left(\hat{\mathbf{X}}^i \parallel \mathbf{K}\right)\right)\right). \quad (15)$$

The final output $\hat{\mathbf{X}}^1$ and $\hat{\mathbf{Y}}^1$ after N reverse SACBs are transformed back to spatial domain to generate the recovery image $\hat{\mathbf{x}}$ along with a recovery byproduct $\hat{\mathbf{y}}$:

$$\hat{\mathbf{x}} = \text{IWT}(\hat{\mathbf{X}}^1), \quad (16)$$

$$\hat{\mathbf{y}} = \text{IWT}(\hat{\mathbf{Y}}^1). \quad (17)$$

If any different secret key \tilde{k} is used in the above recovery procedure, only a wrong recovery image $\tilde{\mathbf{x}}$ will be produced. In both correct or wrong recovery cases, the recovery by-product ($\tilde{\mathbf{y}}$ or $\tilde{\mathbf{y}}$) should not disclose the original face in clear form.

D. Wrong Recovery Modes

As no reference signal is available to directly supervise the generation of wrong recovery images, it is not trivial to define what the wrong recovery image should look like. Therefore, we devise two modes of wrong recovery within the framework to tackle malicious recovery attempts in different scenarios:

1) **Randomized Wrong Recovery (RandWR):** In the RandWR mode, any wrong recovery image presents highly randomized visual patterns, distinguishable from either the original or the pre-obfuscated images significantly. It is hardly possible to observe any meaningful visual features about the original face in the wrong recovery image within this mode. This is to simulate the incorrect decryption effect in cryptography where any mistake in the secret key should lead to totally random decryption results (aka the *avalanche effect*).

2) **Obfuscated Wrong Recovery (ObfsWR):** In the ObfsWR mode, any wrong recovery image stays in the same visually obfuscated form as the protection image, or the pre-obfuscated one. The benefit of this mode is making a false appearance to attackers that the recovery attempt has never worked, or the protection image is simply an obfuscated one without the capability of being recovered.

The two WR modes are illustrated briefly in Fig. 4. The design of the two modes aims to offer different degrees of confusion to potential malicious recovery attempts. Exclusive training objectives are designed to achieve the objective of

each specific mode (in Section IV-E). The invertible protection network is designed to work in either mode rather than supporting both at the same time. For a model built w.r.t. either WR mode, the correct recovery image using the correct secret key should always be near identical to the original image.

E. Learning Objectives

To guarantee the functioning of the framework, a set of loss functions are designed to optimize the protection and recovery processes mutually with respect to different recovery modes.

1) *Protection Loss*: In the forward protection pass, the following loss is defined to optimize the similarity between the protection image $\hat{\mathbf{y}}$ and the pre-obfuscated image \mathbf{y} :

$$\mathcal{L}_P = \beta \cdot \text{LPIPS}(\hat{\mathbf{y}}, \mathbf{y}) + \|\hat{\mathbf{y}} - \mathbf{y}\|_1, \quad (18)$$

where LPIPS stands for perceptual loss defined by Learned Perceptual Image Patch Similarity [44], $\|\cdot\|_1$ indicates L1 distance, and β is a weight parameter set to 5 empirically.

2) *Recovery Loss*:

a) *Correct recovery loss*: In the recovery pass, we first apply L1 norm to constrain the correct recovery image in pixel level using the correct key applied in protection:

$$\mathcal{L}_R = \|\tilde{\mathbf{x}} - \mathbf{x}\|_1. \quad (19)$$

b) *RandWR loss*: Then, to optimize the functioning of the RandWR mode, where the wrong recovery image is expected to be randomized, we define two special triplet losses to optimize the wrong recovery image simultaneously with the correct recovery image in a contrastive manner:

$$\mathcal{L}_{\text{RandWR}} = \mathcal{L}_{\text{TriLPIPS}}(\mathbf{x}, \tilde{\mathbf{x}}, \tilde{\mathbf{x}}) + \mathcal{L}_{\text{TriL1}}(\mathbf{x}, \tilde{\mathbf{x}}, \tilde{\mathbf{x}}), \quad (20)$$

where $\mathcal{L}_{\text{TriLPIPS}}$ stands for the triplet loss using LPIPS as distance metric with anchor (A), positive (P) and negative (N) defined as follows:

$$\mathcal{L}_{\text{TriLPIPS}}(A, P, N) = \max(\text{LPIPS}(A, P) - \text{LPIPS}(A, N) + 1.0, 0). \quad (21)$$

Accordingly, $\mathcal{L}_{\text{TriL1}}$ stands for similar triplet loss based on L1 norm. The dual triplet losses defined in Eq. (20) aims to push the wrong recovery image away from the original and the correct recovery image in both perceptual and pixel domain, while making the later two stay close. It is meaningful considering no reference signal is directly available for supervising the wrong recovery images in the RandWR mode.

c) *ObfsWR loss*: For the ObfsWR mode, we use the pre-obfuscated image to supervise the wrong recovery image directly, plus dual LPIPS triplet losses to optimize the visual appearance of both correct and wrong recovery images jointly:

$$\mathcal{L}_{\text{ObfsWR}} = \|\tilde{\mathbf{x}} - \mathbf{y}\|_1 + \mathcal{L}_{\text{TriLPIPS}}(\tilde{\mathbf{x}}, \mathbf{y}, \mathbf{x}) + \mathcal{L}_{\text{TriLPIPS}}(\tilde{\mathbf{x}}, \mathbf{x}, \mathbf{y}). \quad (22)$$

3) *The overall loss*: During training, secret keys are sampled at random in the protection pass, and the same set of keys are applied in recovery for computing the correct recovery loss. In parallel, a different set of keys are randomly generated and used in recovery for computing the wrong

recovery loss. Finally, the overall loss function for training the entire framework is formulated as

$$\mathcal{L}_{\text{Total}} = \lambda_1 \mathcal{L}_P + \lambda_2 \mathcal{L}_R + \lambda_3 \mathcal{L}_{\text{WR}}, \quad (23)$$

where \mathcal{L}_{WR} is either $\mathcal{L}_{\text{RandWR}}$ or $\mathcal{L}_{\text{ObfsWR}}$ depending on the wrong recovery mode expected. λ_1 , λ_2 and λ_3 are hyper-parameters for balancing different loss terms.

V. EXPERIMENTS

A. Experimental Settings

1) *Datasets*: Three datasets are used in our experiments:

CelebA [45] is one of the most widely used datasets for face recognition, containing 202'599 celebrity images of 10'177 identities. Each image is annotated with 5 landmarks and 40 binary attributes. The dataset is split in train, valid and test subsets. We use its training and validation splits for training and validating our model, and randomly sample 1'000 images from the testing split for evaluation.

LFW [46] contains more than 13'000 images of 5'749 identities and provides the most widely used benchmark for face verification. We only use a subset of 1K images from this dataset for evaluation.

FFHQ [28] contains 70'000 high-quality face images in resolution up to 1024×1024 . The dataset exhibits diverse ages, ethnicities, backgrounds and accessories, and is widely used in face generation research. Similarly, we randomly sample 1K images from the last 1/10 part of the dataset for testing only.

All images in our experiments are uniformly processed by center cropping and keeping only the facial part. Resolution of 112×112 is used throughout the experiments. The sampling of the 3K test images is based on a fixed random seed such that the exact subset can be reproduced from the original datasets. The entire 3K test set and the sampling script will be made publicly available for future researchers to perform evaluations of the same task at a fair benchmark.

2) *Pre-obfuscators*: To demonstrate the generalization of the proposed framework, we experiment with six visual obfuscators belonging to different types including Gaussian blur, pixelate, median filter, FaceShifter [47], SimSwap [48], and image masking. The former three are typical image filters removing high-frequency visual details, and are by de facto the most widely used methods in practice. FaceShifter and SimSwap are well known face swapping algorithms that replace the identity of the face in image with another one. Image masking means overlaying a cartoon facial sticker on top of the original face.

We randomly vary the type and configuration of obfuscators during training and use a fixed configuration in testing. The specifications of the six obfuscators are given below:

- **Gaussian blur (GB)**: the Gaussian kernel size is fixed to 21 while the sigma value is chosen uniformly at random to lie in range of 6 to 10 during training. In evaluation, the sigma value is fixed to 8.
- **Pixelate (PL)**: the block size for pixelate is chosen uniformly at random between integer 5 and 13 during training. In evaluation, the block size is fixed to 9.

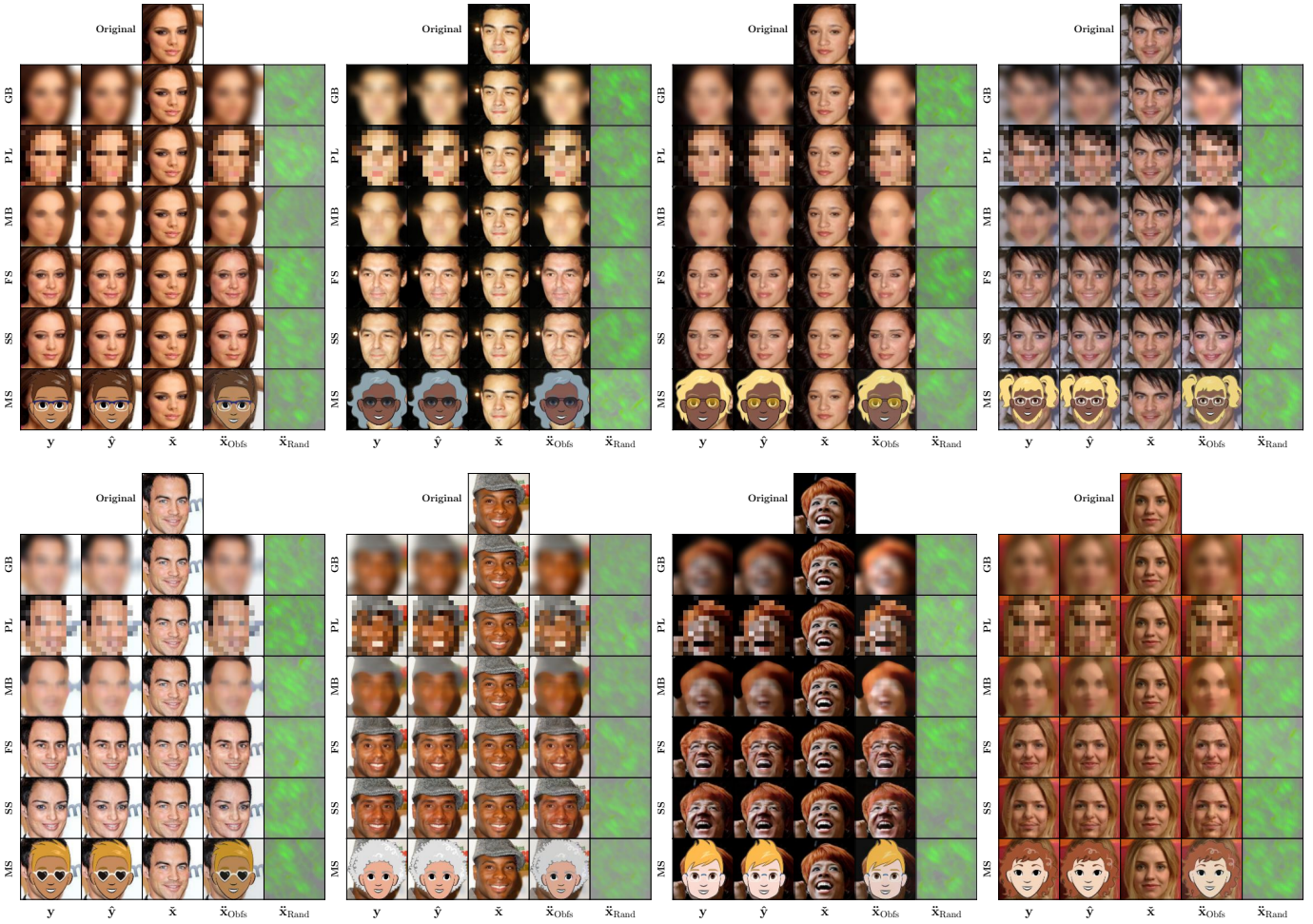


Fig. 5. Image samples (from CelebA) within the PRO-Face S framework. On the top is the original image (\mathbf{x}). Columns from left to right indicate the pre-obfuscated (\mathbf{y}), protected ($\hat{\mathbf{y}}$), correct recovery ($\tilde{\mathbf{x}}$), and wrong recovery image in the ObfsWR ($\tilde{\mathbf{x}}_{\text{Obfs}}$) and the RandWR ($\tilde{\mathbf{x}}_{\text{Rand}}$) modes respectively.

- **Median blur (MB)**: the kernel size of the median filter is chosen uniformly at random between 8 and 22. In evaluation, the median kernel size is fixed to 15.
- **FaceShifter (FS)** [47]: the source identity images for the face swapping algorithm are randomly chosen from a subset of the CelebA [45] test split that exhibit only frontal pose, in both training and testing.
- **SimSwap (SS)** [48]: the same as FaceShifter above.
- **Masking (MS)**: the cartoon face sticker is randomly chosen from the dataset CartoonSet [49] and directly overlaid on the inner part of the original face, in both training and testing.

3) *Metrics*: We utilize three commonly used image similarity metrics (PSNR, SSIM [50] and LPIPS [44]) to measure the quality of privacy protection images, correct recovery images, and the visual discrepancy of the wrong recovery images. Unlike several prior studies where face verification is used to measure visual privacy, we keep using traditional metrics considering face recognition rate does not always comply with human subjective perception towards anonymized face, which has been discussed in [30], [51].

a) *Privacy protection metric*: The visual similarity between the protection and pre-obfuscated images are computed to signal the **relative privacy score**. Note that, since our framework relies on a pre-obfuscator as the protection template, it assumes the privacy is well preserved in the pre-obfuscated image. Therefore, we call it *relative privacy score* as it indicates how the protection image is close the pre-obfuscated template, relatively. Higher similarity metric indicates stronger protection capability.

b) *Correct recovery metric*: The visual similarity between the correct recovery and the original images is computed to signal the quality of image recovery. Higher similarity score indicates superior recovery performance.

c) *Wrong recovery metric*: For wrong image recovery scenarios, we define **wrong recovery discrepancy** of wrong recovery images under each WR mode as follows: For RandWR, the discrepancy is computed as the similarity between the wrong recovery and the original images, which is expected to be low; For ObfsWR, the similarity metrics between the wrong recovery and the pre-obfuscated images are computed and expected to be high.

TABLE I

RELATIVE PRIVACY PROTECTION PERFORMANCE IN TERMS OF PSNR, SSIM AND LPIPS BETWEEN PROTECTION AND PRE-OBFUSCATION IMAGES, MEASURED ON THE TEST SET OF LFW, CELEBA AND FFHQ. BOLD AND UNDERLINED NUMBERS INDICATE THE BEST AND THE SECOND BEST SCORES OVER EACH COLUMN WHEN COMPARING OUR AVERAGED RESULTS (AVG.) WITH THE OTHER TWO COMPETITORS.

Methods		LFW			CelebA			FFHQ		
		PSNR \uparrow	SSIM \uparrow	LPIPS \downarrow	PSNR \uparrow	SSIM \uparrow	LPIPS \downarrow	PSNR \uparrow	SSIM \uparrow	LPIPS \downarrow
<i>Competitors</i>	PRO-Face [30]	34.77	0.973	0.0261	34.95	0.969	0.0206	34.68	0.966	0.0253
	IMN [31]	48.79	<u>0.989</u>	0.0079	48.57	<u>0.988</u>	0.0081	48.97	0.991	0.0068
		<u>44.92</u>	0.990	0.0001	<u>43.81</u>	0.989	0.0001	<u>43.17</u>	<u>0.988</u>	0.0001
		39.14	0.975	<u>0.0005</u>	38.20	0.971	<u>0.0006</u>	38.08	0.970	<u>0.0007</u>
		46.64	0.991	0.0	45.25	0.987	0.0001	45.11	0.986	0.0001
		44.1	0.992	0.0001	43.23	0.99	0.0001	42.82	0.989	0.0001
		44.81	0.991	0.0001	43.85	0.988	0.0001	43.52	0.987	0.0001
		47.87	0.996	0.0	46.4	0.996	0.0	45.04	0.994	0.0001
<i>PRO-Face S</i>	RandWR (SS)	47.97	0.997	0.0	46.31	0.996	0.0	44.89	0.995	0.0001
	RandWR (MS)	38.11	0.975	0.0002	37.8	0.973	0.0002	37.66	0.973	0.0002
		42.1	0.974	0.0003	41.14	0.968	0.0004	41.11	0.967	0.0005
		38.92	0.979	0.0006	38.15	0.975	0.0007	38.13	0.974	0.0007
		40.3	0.976	0.0005	39.47	0.97	0.0006	39.51	0.969	0.0007
		40.99	0.986	0.0003	39.72	0.984	0.0004	39.42	0.982	0.0005
		40.83	0.986	0.0003	39.27	0.985	0.0004	39.01	0.983	0.0004
		31.69	0.947	0.001	31.43	0.943	0.0011	31.32	0.943	0.0012

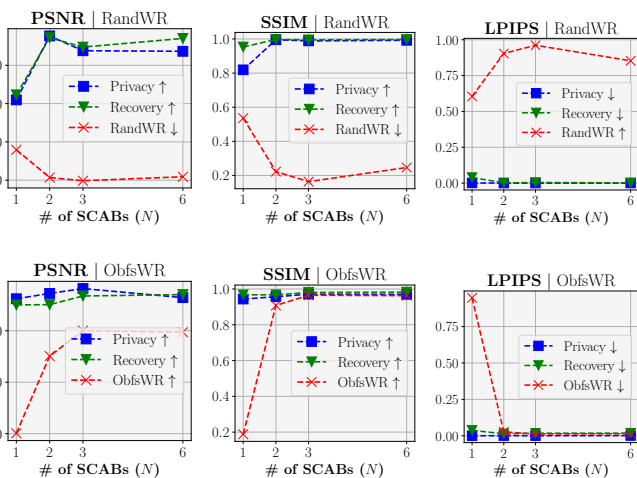


Fig. 6. Protection and recovery performance on CelebA measured by PSNR, SSIM and LPIPS versus the number of SACBs.

4) *Implementation details:* All experiments are performed on a single NVIDIA GeForce RTX 3090 GPU. The Adam optimizer with $\beta_1 = 0.9$ and $\beta_2 = 0.999$ is used in training. A small learning rate of 0.00001 is applied to avoid the vanishing gradient problem of INN. The training batch size is set to 12. We experiment with different values of the hyper-parameter N (the number of SACBs) and finally use $N=3$ as it achieves the optimal overall performance (see Figure 6) with relatively lightweight model size. The entire training process takes more than 135,000 steps to stabilize, which lasts approximately 12 hours. A visualization of several protection and recovery examples using different obfuscators is presented in Figure 5.

B. Evaluation of Privacy Protection

To evaluate privacy, we compare with another two solutions employing the similar methodology of template-based

protection, i.e., PRO-Face [30] and IMN [31]. Table I shows the privacy scores of multiple cases: for PRO-Face [30], the average scores over different obfuscators are shown; for IMN [31], SimSwap is used as the paper claims; in our case, the average scores over different obfuscators and the scores corresponding to each obfuscator are shown. It is clear that our approach outperforms PRO-Face with large margin in most cases and metrics. This is because PRO-Face aims to preserve identifiable information in the protected images and therefore sacrifices visual privacy. Compared with IMN [31], our framework built with the RandWR mode performs slightly better in terms of SSIM and LPIPS. In the ObsfWR mode, our performance is slightly reduced, but still shows better LPIPS score than IMN [31]. Nevertheless, we consider the difference between our approach and IMN is extremely subtle, and both should be considered as near lossless visual quality. Considering our framework is with secure reversibility and is much more lightweight (verified in Section V-E), we claim to achieve a meaningful improvement over the state-of-the-art approach IMN [31]. Several protection samples with SimSwap as pre-obfuscator by different methods are visualized in Figure 7. The performance of PRO-Face [30] is visibly insufficient compared to ours. While, both IMN [31] and ours are with excellent performance in terms of high visual similarity with SwimSwap obfuscation.

When inspecting the privacy scores with respect to each obfuscator, it is obvious that FaceShifter and SimSwap perform slightly better, whereas Masking ranks the last. This might be because Cartoon sticker masked on the original face introduces much domain shift different from others, while face swapping still presents natural facial appearances. Nevertheless, such a difference in quality metrics is still subtle.

C. Evaluation of Reversibility

We then evaluate the reversibility of our framework, in terms of the correct recovery and wrong recovery performance.

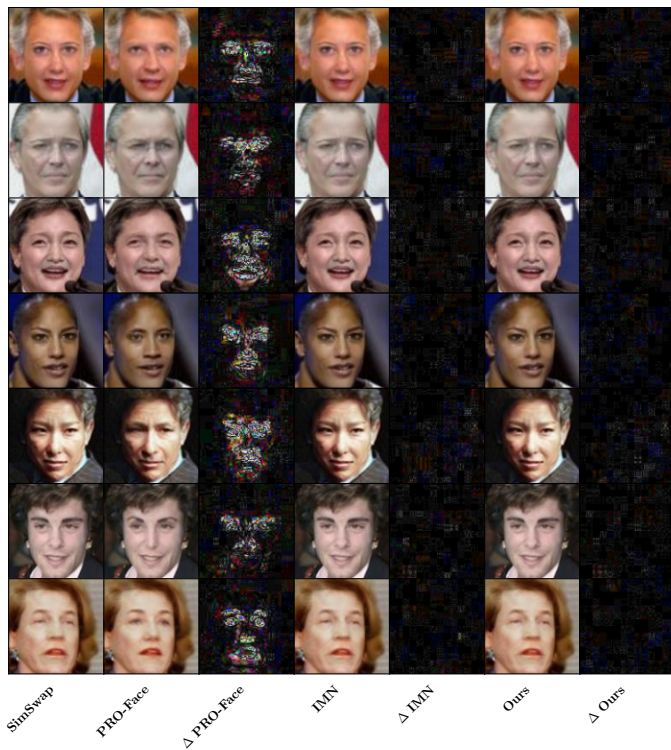


Fig. 7. Protection samples (from LFW) based on SimSwap as pre-obfuscator for different methods. Δ indicates $10\times$ magnified absolute difference image between the protection image and the SimSwap template.

1) *Correct recovery performance*: In the scenario of correct image recovery, the recovery scores for different methods are shown in Table II. One easily observes the significant improvements of our approach over most other competitors. Compared with IMN [31], our approach again exhibits comparable recovery performance with slightly improved SSIM and LPIPS in the RandWR mode. The correct recovery in the mode of ObfsWR is slightly reduced but still keeps high quality in terms of perceptual quality ($\text{PSNR} > 35\text{dB}$ and $\text{SSIM} > 0.97$). Again, we visualize in Fig. 8 correct recovery samples of Gu [18], IMN [31] and ours, including the difference image between the correct recovery and the original image. It is clear that our approach outperforms Gu [18] by presenting more precise reconstruction of color intensity and facial details, whereas IMN [31] shows comparable visual quality as ours.

2) *Wrong recovery performance*: In the scenario of wrong image recovery, the wrong recovery discrepancy scores for the two distinct modes respect to different obfuscators are listed in Table III. In the RandWR mode, the discrepancy score stays in a low level as expected, with SSIM below 0.2 and LPIPS well above 0.9. In the ObfsWR mode, the discrepancy score remains high, indicating the success of keeping wrong recovery images obfuscated.

Once again, the similar trend is found when comparing over obfuscators, where Masking performs less sufficiently due to the domain difference induced by the cartoon sticker.

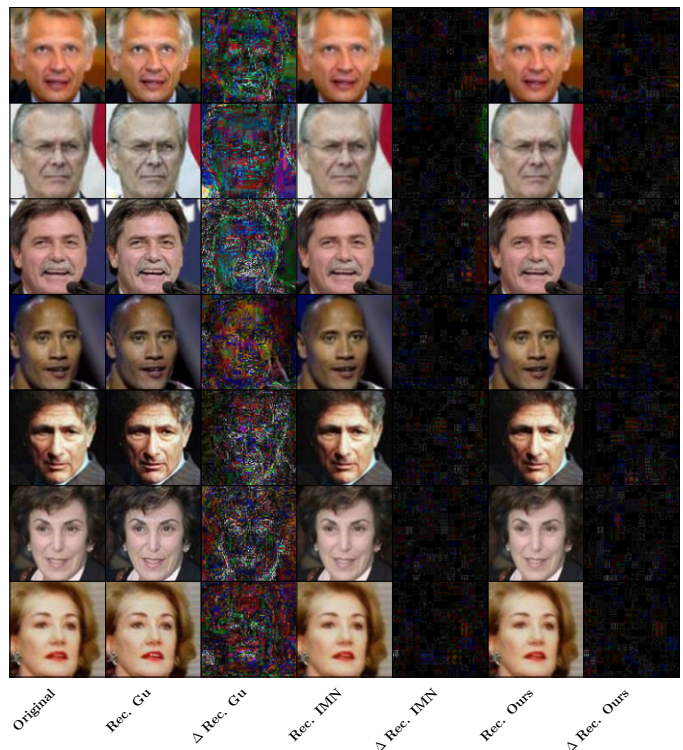


Fig. 8. Recovery samples (from LFW) of different methods, where Δ Rec. indicates $10\times$ magnified absolute difference image between the correct recovery image and the original image.

D. Security Analysis

Since PRO-Face S does not claim to offer rigorous security as cryptography, we analyze the security of the proposed framework in an empirical and qualitative way from the following two aspects:

1) *Malicious recovery attempts*: We first experiment with “malicious” recovery attempts using wrong secret keys or by substituting the protection image with the pre-obfuscated one to simulate a kind of “spoofing attack”. Several wrong recovery samples under the two cases are shown in Fig. 9a. It is obvious that the recovery still fails even with 1-bit difference in the secret key, for both RandWR and ObfsWR cases. When presenting the pre-obfuscated image to the recovery module, it is still hard to recover the correct image although the pre-obfuscated image is highly similar to the protection image. In practice, this feature allows us to apply the full protection procedure only on a few key video frames while keeping the other frames in pre-obfuscated form, similar as PECAM [20]. It will not only reduce computational burdens but also confuse potential attackers.

2) *Byproduct analysis*: We also analyze the security risks potentially existing in the byproduct images generated along protection and recovery, which has never been thoroughly investigated in prior studies employing the similar methodologies, e.g., IMN [31]. Hereby, we visualize in Fig. 9b several samples of the protection byproduct \hat{x} , and the recovery byproduct in both correct and wrong recovery cases, i.e., $\hat{y}_{\text{Rand/Obfs}}$ and $\check{y}_{\text{Rand/Obfs}}$. It is clear that any byproduct image generated in the recovery stage does not disclose the

TABLE II

CORRECT RECOVERY SCORES IN TERMS OF PSNR, SSIM AND LPIPS. BOLD AND UNDERLINED NUMBERS INDICATE THE BEST AND THE SECOND BEST SCORES OVER EACH COLUMN WHEN COMPARING OUR AVG. RESULTS WITH THE OTHER COMPETITORS. *WE QUOTE THE RECOVERY SCORES FROM THE PUBLISHED VERSION OF CAO [19] AND RAPP [26] ON CELEBA SINCE NO OPEN SOURCE IMPLEMENTATION IS AVAILABLE.

Methods		LFW			CelebA			FFHQ		
		PSNR \uparrow	SSIM \uparrow	LPIPS \downarrow	PSNR \uparrow	SSIM \uparrow	LPIPS \downarrow	PSNR \uparrow	SSIM \uparrow	LPIPS \downarrow
Competitors	Gu [18]	30.8	0.938	0.0632	30.52	0.932	0.0682	28.16	0.921	0.0875
	Cao [19]*	—	—	—	27.5	0.902	0.062	—	—	—
	RAPP [26]*	—	—	—	29.06	0.809	0.057	—	—	—
	RiDDLE (e2e) [27]	21.65	0.789	0.2213	19.19	0.714	0.2285	20.56	0.749	0.2591
	RiDDLE (latent) [27]	27.14	0.921	0.0941	26.2	0.9	0.089	27.14	0.921	0.0941
	IMN [31]	49.1	<u>0.995</u>	0.0210	49.14	<u>0.995</u>	<u>0.0175</u>	48.83	0.995	<u>0.0172</u>
RandWR (Avg.)		<u>46.87</u>	0.998	0.0044	<u>44.76</u>	0.997	0.0043	<u>41.14</u>	<u>0.990</u>	0.0061
ObfsWR (Avg.)		37.95	0.985	<u>0.0170</u>	36.76	0.981	0.0176	35.86	0.977	0.0194
PRO-Face S	RandWR (GB)	49.18	0.998	0.0009	46.37	0.997	0.0014	42.03	0.992	0.0031
	RandWR (PL)	46.91	0.997	0.0021	44.9	0.996	0.0024	41.19	0.991	0.0044
	RandWR (MB)	44.36	0.998	0.0079	42.98	0.996	0.0067	40.3	0.992	0.0073
	RandWR (FS)	49.49	0.998	0.0009	46.77	0.997	0.0013	42.25	0.993	0.0031
	RandWR (SS)	49.05	0.998	0.001	46.27	0.997	0.0015	41.87	0.992	0.0034
	RandWR (MS)	42.2	0.987	0.0139	41.26	0.986	0.0127	39.22	0.981	0.0153
	ObfsWR (GB)	37.7	0.984	0.0167	36.06	0.977	0.0191	35.3	0.975	0.022
	ObfsWR (PL)	38.82	0.985	0.0149	37.52	0.982	0.016	36.43	0.978	0.0178
	ObfsWR (MB)	37.5	0.984	0.0191	35.95	0.978	0.0215	35.18	0.975	0.0238
	ObfsWR (FS)	38.13	0.986	0.017	37.33	0.984	0.0163	36.31	0.98	0.0166
	ObfsWR (SS)	38.13	0.988	0.018	37.08	0.985	0.0177	36.12	0.981	0.0196
	ObfsWR (MS)	37.41	0.98	0.0159	36.64	0.978	0.0152	35.8	0.975	0.0165

TABLE III

WRONG RECOVERY DISCREPANCY IN TERMS OF PSNR, SSIM AND LPIPS WITH RESPECT TO DIFFERENT WR MODES AND OBFUSCATORS.

WR mode / Obf.		LFW			CelebA			FFHQ		
		PSNR \downarrow	SSIM \downarrow	LPIPS \uparrow	PSNR \downarrow	SSIM \downarrow	LPIPS \uparrow	PSNR \downarrow	SSIM \downarrow	LPIPS \uparrow
RandWR	Avg.	10.45	0.183	0.9454	9.86	0.164	0.9616	10.53	0.186	0.9988
	GB	10.44	0.179	0.9494	9.86	0.16	0.9680	10.54	0.183	1.0037
	PL	10.46	0.183	0.9454	9.89	0.165	0.9603	10.53	0.184	0.9997
	MB	10.45	0.179	0.9489	9.86	0.161	0.9650	10.51	0.183	1.0027
	FS	10.47	0.182	0.9465	9.87	0.163	0.9617	10.56	0.186	0.9993
	SS	10.47	0.182	0.9467	9.86	0.163	0.9628	10.53	0.184	1.0011
	MS	10.39	0.192	0.9355	9.8	0.171	0.952	10.54	0.198	0.9864
ObfsWR	Avg.	28.97	0.968	0.0147	30.03	0.965	0.0122	28.76	0.971	0.0153
	GB	24.57	0.966	0.0281	27.03	0.969	0.0212	25.49	0.969	0.0291
	PL	28.57	0.963	0.0102	29.73	0.959	0.0085	28.36	0.969	0.0103
	MB	25.39	0.96	0.021	27.65	0.960	0.0168	25.9	0.965	0.0212
	FS	33.64	0.977	0.0095	34.10	0.970	0.0082	32.48	0.982	0.0104
	SS	34.55	0.985	0.0097	34.82	0.982	0.0088	33.3	0.986	0.0094
	MS	27.12	0.955	0.0098	26.83	0.949	0.01	27.02	0.957	0.0115

original face in clear form. However, we do recognize the risk existing in the byproduct \hat{x} generated along protection, which reveals certain level visual information about the original face, especially with the blur-based obfuscators (marked in red rectangle). Considering the protection byproduct output is not required for recovery, it should be discarded immediately upon generation to minimize the privacy risks.

E. Complexity and Cost

To demonstrate the lightweight of our framework, we summarize the number of model parameters and the inference time for multiple reversible solutions in Table V. Image size and batch size are uniformly set to 112×112 and 16 for a fair comparison. For PRO-Face S and IMN [31], we count only the

model size of the invertible network without considering the pre-obfuscation model. It is clear that PRO-Face S possesses the minimum number of model parameters ($\sim 1M$) among the all. As for the time cost, it takes only 0.014 seconds per batch for our framework to finish a full protection operation using Gaussian blur as pre-obfuscator. When using the more sophisticated SimSwap, the inference time is increased to 0.595 seconds but still well below the other competitors. Therefore, we claim the proposed framework is lightweight yet offering the optimal overall performance.

F. Ablation Study

Last but not least, we carry out the ablation study to verify the effectiveness of several key components of the

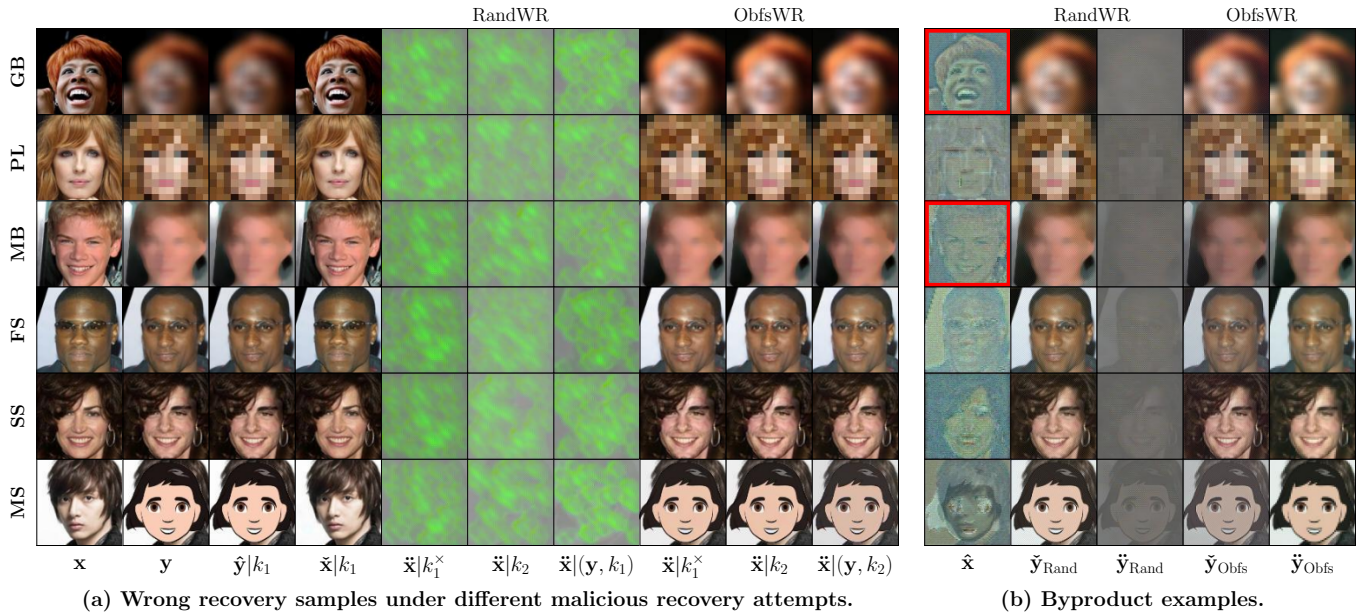


Fig. 9. Image samples (from FFHQ) illustrating (a) wrong recovery under various malicious recovery attempts, and (b) byproducts generated within the framework. k_1^x denotes a secret key that has only 1-bit difference from k_1 , and k_2 denotes a random secret key significantly different from k_1 .

TABLE IV
RESULTS OF THE ABLATION STUDY ON PRIVACY PROTECTION, CORRECT AND WRONG RECOVERIES WITH RESPECT TO DIFFERENT FRAMEWORK VARIATIONS. THE NUMBERS IN BOLD INDICATE THE BEST SCORE OVER EACH COLUMN.

	Privacy protection			Correct recovery			RandWR			ObfsWR		
	PSNR \uparrow	SSIM \uparrow	LPIPS \downarrow	PSNR \uparrow	SSIM \uparrow	LPIPS \downarrow	PSNR \downarrow	SSIM \downarrow	LPIPS \uparrow	PSNR \uparrow	SSIM \uparrow	LPIPS \downarrow
w/o \mathcal{L}_{TriL1}	41.70	0.985	0.0004	43.34	0.992	0.0045	10.68	0.284	0.7866	—	—	—
w/o $\mathcal{L}_{TriLPIPS}$	39.76	0.934	0.0021	41.01	0.946	0.0137	—	—	—	28.61	0.923	0.0201
w/o \mathbf{K} in rec.	42.36	0.984	0.0001	42.03	0.990	0.0084	10.12	0.252	0.828	29.68	0.961	0.0131
Full	43.81	0.989	0.0001	44.76	0.995	0.0043	9.86	0.164	0.9616	30.03	0.965	0.0122

proposed framework. Instead of checking the effectiveness of the DWT/IWT modules and the DenseNet structure in the INN that have been well investigated in [31], [42], we analyze the functionality of several unique components introduced in the PRO-Face S: The first variation is the triplet loss \mathcal{L}_{TriL1} defined in Eq. (20) for RandWR mode optimization; The second are the two perceptual triplet losses $\mathcal{L}_{TriLPIPS}$ specified in Eq. (22) for the ObfsWR mode; Another variation is the use of the secret map \mathbf{K} as input of recovery instead of using Gaussian noise as [31], [42]. We train and test the framework by removing each of those variations and report the performance on CelebA in Table IV. It is quite clear that our final configuration integrating all above variations offers the optimal overall performance, which verifies the effectiveness of each introduced component.

VI. CONCLUSION

This paper proposes **PRO-Face S**, a unified framework for Privacy-preserving Reversible Obfuscation of Face images via Secure flow-based model. The framework elegantly assembles multiple merits that a visual privacy protection solution should have, including higher diversity supporting different types of obfuscation, personalized anonymity powered by use-specified obfuscator, near lossless image recovery thanks to

TABLE V
STORAGE AND TIME COST OF DIFFERENT REVERSIBLE SOLUTIONS.

Metric	PRO-Face S	IMN [31]	Gu [18]	Riddle [27]
# params	1.07M	4.05M	11.43M	40.03M
s/batch	min 0.014 / max 0.595	1.84	1.229	2.49

INN, security against different malicious recovery attempts, and yet lightweight model allowing for more practical applications. Extensive experiments and comprehensive analysis demonstrate the effectiveness of the proposed framework in privacy protection, image recovery and empirical security enforcement.

Yet, certain limitations still remain, which have not been addressed in our work. For instance, we make a strong assumption that the pre-obfuscated image is privacy-free, which is not always true as the obfuscated image may still be inverted to clear form by image enhancement. The recovery robustness against commonly used image processing (such as JPEG) applied on the protection image is still an open question. Moreover, it is ideal to solve the privacy risk related to the protection byproduct mentioned in Section V-D2 to build a more secure framework. Those will serve as our future work.

REFERENCES

- [1] Kashmir Hill, “The Secretive Company That Might End Privacy as We Know It,” <https://www.nytimes.com/2020/01/18/technology/clearview-privacy-facial-recognition.html>, 2020, The New York Times.
- [2] William Turton, “Hackers Breach Thousands of Security Cameras, Exposing Tesla, Jails, Hospitals,” <https://finance.yahoo.com/news/hackers-breach-thousands-security-cameras-213219424.html>, 2021, Bloomberg.
- [3] Wu Lei, “China’s first lawsuit on facial recognition made verdict,” http://www.ehangzhou.gov.cn/2021-04/12/c_276775.htm, 2021, China Global Television Network (CGNT).
- [4] A. Erdélyi, T. Barát, P. Valet, T. Winkler, and B. Rinner, “Adaptive Cartooning for Privacy Protection in Camera Networks,” in *2014 11th IEEE International Conference on Advanced Video and Signal Based Surveillance (AVSS)*, 2014, pp. 44–49.
- [5] L. Yuan and T. Ebrahimi, “Image Privacy Protection with Secure JPEG Transmorphism,” *IET Signal Processing*, vol. 11, no. 9, pp. 1031–1038, 2017.
- [6] P. Korshunov and T. Ebrahimi, “Using Warping for Privacy Protection in Video Surveillance,” in *2013 18th International Conference on Digital Signal Processing (DSP)*, 2013, pp. 1–6.
- [7] B. Meden, P. Rot, P. Terhórst, N. Damer, A. Kuijper, W. J. Scheirer, A. Ross, P. Peer, and V. Štruc, “Privacy-Enhancing Face Biometrics: A Comprehensive Survey,” *IEEE Transactions on Information Forensics and Security (TIFS)*, vol. 16, pp. 4147–4183, 2021.
- [8] J. Zhou and C.-M. Pun, “Personal Privacy Protection via Irrelevant Faces Tracking and Pixelation in Video Live Streaming,” *IEEE Transactions on Information Forensics and Security (TIFS)*, vol. 16, pp. 1088–1103, 2021.
- [9] S. Çiftçi, A. O. Akyüz, and T. Ebrahimi, “A reliable and reversible image privacy protection based on false colors,” *IEEE Transactions on Multimedia (TMM)*, vol. 20, no. 1, pp. 68–81, 2018.
- [10] V. Mirjalili, S. Raschka, and A. Ross, “PrivacyNet: Semi-Adversarial Networks for Multi-Attribute Face Privacy,” *IEEE Transactions on Image Processing (TIP)*, vol. 29, pp. 9400–9412, 2020.
- [11] S. J. Oh, M. Fritz, and B. Schiele, “Adversarial Image Perturbation for Privacy Protection A Game Theory Perspective,” in *2017 IEEE International Conference on Computer Vision (ICCV 2017)*, 2017, pp. 1491–1500.
- [12] S. Shan, E. Wenger, J. Zhang, H. Li, H. Zheng, and B. Y. Zhao, “Fawkes: Protecting Privacy against Unauthorized Deep Learning Models,” in *29th USENIX Security Symposium (USENIX Security)*, 2020, pp. 1589–1604.
- [13] S. Hu, X. Liu, Y. Zhang, M. Li, L. Y. Zhang, H. Jin, and L. Wu, “Protecting Facial Privacy: Generating Adversarial Identity Masks via Style-robust Makeup Transfer,” in *2022 IEEE/CVF Conference on Computer Vision and Pattern Recognition (CVPR 2022)*, 2022.
- [14] Q. Sun, L. Ma, S. Joon Oh, L. V. Gool, B. Schiele, and M. Fritz, “Natural and Effective Obfuscation by Head Inpainting,” in *2018 IEEE/CVF Conference on Computer Vision and Pattern Recognition (CVPR 2018)*, 2018, pp. 5050–5059.
- [15] H. Hukkelás, R. Mester, and F. Lindseth, “DeepPrivacy: A Generative Adversarial Network for Face Anonymization,” in *International Symposium on Visual Computing (ISVC 2019)*, 2019, pp. 565–578.
- [16] O. Gafni, L. Wolf, and Y. Taigman, “Live Face De-Identification in Video,” in *IEEE/CVF International Conference on Computer Vision (ICCV 2019)*, vol. 00, 2019, pp. 9377–9386.
- [17] M. Maximov, I. Elezi, and L. Leal-Taixé, “CIAGAN: Conditional Identity Anonymization Generative Adversarial Networks,” in *2020 IEEE/CVF Conference on Computer Vision and Pattern Recognition (CVPR 2020)*, vol. 00, 2020, pp. 5446–5455.
- [18] X. Gu, W. Luo, M. S. Ryoo, and Y. J. Lee, “Password-Conditioned Anonymization and De-anonymization with Face Identity Transformers,” in *European Conference on Computer Vision (ECCV 2020)*, 2020, pp. 727–743.
- [19] J. Cao, B. Liu, Y. Wen, R. Xie, and L. Song, “Personalized and Invertible Face De-Identification by Disentangled Identity Information Manipulation,” in *Proceedings of the IEEE/CVF International Conference on Computer Vision (ICCV 2021)*, 2021, pp. 3334–3342.
- [20] H. Wu, X. Tian, M. Li, Y. Liu, G. Ananthanarayanan, F. Xu, and S. Zhong, “PECAM: Privacy-Enhanced Video Streaming and Analytics via Securely-Reversible Transformation.” New York, NY, USA: Association for Computing Machinery, 2021.
- [21] J. Li, L. Han, R. Chen, H. Zhang, B. Han, L. Wang, and X. Cao, “Identity-Preserving Face Anonymization via Adaptively Facial Attributes Obfuscation,” in *Proceedings of the 29th ACM International Conference on Multimedia (MM 2021)*, 2021, p. 3891–3899.
- [22] J. Li, H. Zhang, S. Liang, P. Dai, and X. Cao, “Privacy-Enhancing Face Obfuscation Guided by Semantic-Aware Attribution Maps,” *IEEE Transactions on Information Forensics and Security*, vol. 18, pp. 3632–3646, 2023.
- [23] H. Proença, “The UU-Net: Reversible Face De-Identification for Visual Surveillance Video Footage,” *IEEE Transactions on Circuits and Systems for Video Technology*, vol. 32, no. 2, pp. 496–509, 2022.
- [24] Z. Yuan, Z. You, S. Li, Z. Qian, X. Zhang, and A. Kot, “On generating identifiable virtual faces.” New York, NY, USA: Association for Computing Machinery, 2022.
- [25] Y. Wen, B. Liu, J. Cao, R. Xie, L. Song, and Z. Li, “IdentityMask: Deep Motion Flow Guided Reversible Face Video De-Identification,” *IEEE Transactions on Circuits and Systems for Video Technology (TCSVT)*, vol. 32, no. 12, pp. 8353–8367, 2022.
- [26] Y. Zhang, T. Wang, R. Zhao, W. Wen, and Y. Zhu, “RAPP: Reversible Privacy Preservation for Various Face Attributes,” *IEEE Transactions on Information Forensics and Security (TIFS)*, vol. 18, pp. 3074–3087, 2023.
- [27] D. Li, W. Wang, K. Zhao, J. Dong, and T. Tan, “RiDDLE: Reversible and Diversified De-identification with Latent Encryptor,” in *Proceedings of the IEEE Conference on Computer Vision and Pattern Recognition (CVPR)*, June 2023.
- [28] T. Karras, S. Laine, and T. Aila, “A Style-Based Generator Architecture for Generative Adversarial Networks,” in *2019 IEEE/CVF Conference on Computer Vision and Pattern Recognition (CVPR)*, 2019, pp. 4396–4405.
- [29] Z. You, S. Li, Z. Qian, and X. Zhang, “Reversible Privacy-Preserving Recognition,” in *2021 IEEE International Conference on Multimedia and Expo (ICME)*, 2021, pp. 1–6.
- [30] L. Yuan, L. Liu, X. Pu, Z. Li, H. Li, and X. Gao, “PRO-Face: A Generic Framework for Privacy-Preserving Recognizable Obfuscation of Face Images,” in *Proceedings of the 30th ACM International Conference on Multimedia (MM ’22)*, 2022, p. 1661–1669.
- [31] Y. Yang, Y. Huang, M. Shi, K. Chen, and W. Zhang, “Invertible Mask Network for Face Privacy Preservation,” *Information Sciences*, vol. 629, pp. 566–579, 2023.
- [32] L. Dinh, D. Krueger, and Y. Bengio, “NICE: Non-linear Independent Components Estimation,” in *Workshop of International Conference on Learning Representations, ICLR 2015*.
- [33] L. Dinh, J. Sohl-Dickstein, and S. Bengio, “Density estimation using Real NVP,” in *International Conference on Learning Representations, ICLR 2017*, 2017.
- [34] D. P. Kingma and P. Dhariwal, “Glow: Generative Flow with Invertible 1x1 Convolutions,” in *Advances in Neural Information Processing Systems*, S. Bengio, H. Wallach, H. Larochelle, K. Grauman, N. Cesa-Bianchi, and R. Garnett, Eds. Curran Associates, Inc.
- [35] T. F. van der Ouderaa and D. E. Worrall, “Reversible GANs for Memory-Efficient Image-To-Image Translation,” in *2019 IEEE/CVF Conference on Computer Vision and Pattern Recognition (CVPR)*, 2019, pp. 4715–4723.
- [36] L. Ardizzone, J. Kruse, C. Lüth, N. Bracher, C. Rother, and U. Köthe, “Conditional Invertible Neural Networks for Diverse Image-to-Image Translation,” in *Pattern Recognition*, Z. Akata, A. Geiger, and T. Sattler, Eds. Cham: Springer International Publishing, 2021, pp. 373–387.
- [37] M. Xiao, S. Zheng, C. Liu, Y. Wang, D. He, G. Ke, J. Bian, Z. Lin, and T.-Y. Liu, “Invertible Image Rescaling.” Berlin, Heidelberg: Springer-Verlag, 2020.
- [38] A. Lugmayr, M. Danelljan, L. Van Gool, and R. Timofte, “SRFlow: Learning the Super-Resolution Space with Normalizing Flow.” Berlin, Heidelberg: Springer-Verlag, 2020.
- [39] Y. Liu, Z. Qin, S. Anwar, P. Ji, D. Kim, S. Caldwell, and T. Gedeon, “Invertible Denoising Network: A Light Solution for Real Noise Removal,” in *2021 IEEE/CVF Conference on Computer Vision and Pattern Recognition (CVPR)*, 2021, pp. 13 360–13 369.
- [40] Y. Xie, K. L. Cheng, and Q. Chen, “Enhanced Invertible Encoding for Learned Image Compression.” New York, NY, USA: Association for Computing Machinery, 2021.
- [41] J. Jing, X. Deng, M. Xu, J. Wang, and Z. Guan, “HiNet: Deep Image Hiding by Invertible Network,” in *2021 IEEE/CVF International Conference on Computer Vision (ICCV)*, 2021, pp. 4713–4722.
- [42] Z. Guan, J. Jing, X. Deng, M. Xu, L. Jiang, Z. Zhang, and Y. Li, “DeepMIH: Deep Invertible Network for Multiple Image Hiding,” *IEEE Transactions on Pattern Analysis and Machine Intelligence*, vol. 45, no. 1, pp. 372–390, 2023.
- [43] X. Wang, K. Yu, S. Wu, J. Gu, Y. Liu, C. Dong, Y. Qiao, and C. C. Loy, “ESRGAN: Enhanced Super-Resolution Generative Adversarial Networks.” Berlin, Heidelberg: Springer-Verlag, 2019.

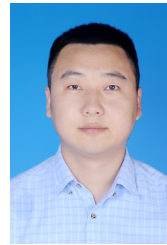
- [44] R. Zhang, P. Isola, A. A. Efros, E. Shechtman, and O. Wang, "The Unreasonable Effectiveness of Deep Features as a Perceptual Metric," in *2018 IEEE/CVF Conference on Computer Vision and Pattern Recognition (CVPR 2018)*, 2018, pp. 586–595.
- [45] Z. Liu, P. Luo, X. Wang, and X. Tang, "Deep Learning Face Attributes in the Wild," in *2015 IEEE International Conference on Computer Vision (ICCV 2015)*, 2015, pp. 3730–3738.
- [46] G. B. Huang, M. Ramesh, T. Berg, and E. Learned-Miller, "Labeled Faces in the Wild: A Database for Studying Face Recognition in Unconstrained Environments," University of Massachusetts, Amherst, Tech. Rep. 07-49, October 2007.
- [47] L. Li, J. Bao, H. Yang, D. Chen, and F. Wen, "Advancing High Fidelity Identity Swapping for Forgery Detection," in *2020 IEEE/CVF Conference on Computer Vision and Pattern Recognition (CVPR 2020)*, 2020, pp. 5073–5082.
- [48] R. Chen, X. Chen, B. Ni, and Y. Ge, "SimSwap: An Efficient Framework For High Fidelity Face Swapping," in *Proceedings of the 28th ACM International Conference on Multimedia (MM 2020)*, 2020, p. 2003–2011.
- [49] A. Royer, K. Bousmalis, S. Gouws, F. Bertsch, I. Mosseri, F. Cole, and K. Murphy, *XGAN: Unsupervised Image-to-Image Translation for Many-to-Many Mappings*. Cham: Springer International Publishing, 2020, pp. 33–49.
- [50] Z. Wang, A. Bovik, H. Sheikh, and E. Simoncelli, "Image Quality Assessment: From Error Visibility to Structural Similarity," *IEEE Transactions on Image Processing (TIP)*, vol. 13, no. 4, pp. 600–612, 2004.
- [51] P. J. Phillips, A. N. Yates, Y. Hu, C. A. Hahn, E. Noyes, K. Jackson, J. G. Cavazos, G. Jeckeln, R. Ranjan, S. Sankaranarayanan, J.-C. Chen, C. D. Castillo, R. Chellappa, D. White, and A. J. O'Toole, "Face recognition accuracy of forensic examiners, superrecognizers, and face recognition algorithms," *Proceedings of the National Academy of Sciences (PNAS)*, vol. 115, no. 24, pp. 6171–6176, 2018.



Yan Zhang received the B.E. degree from National University of Defense Technology, Changsha, China, in 2014, and the M.S. degree from the University of Birmingham, United Kingdom, in 2017, and the Ph.D. degree from Chongqing University, Chongqing, China, in 2020. He is currently a lecturer in Chongqing University of Posts and Telecommunications. His research area includes image processing, machine learning, and pattern recognition.



Jiayu Leng Jiayu Leng received the Ph.D. degree in computer science at University of Chinese Academy of Sciences, Beijing, China, in 2020. He is currently working at School of Computer Science and Technology, Chongqing University of Posts and Telecommunications. His current research interests include computer vision, video anomaly detection, and object detection.



Tao Wu is currently a Professor at the School of CyberSecurity and Information Law, Chongqing University of Posts and Telecommunications, China. He is the Executive Deputy Director of Chongqing Network and Information Security Technology Engineering Laboratory. He received the Ph.D. degree from University of Electronic Science and Technology of China, in June 2017. His research interests include graph neural networks, artificial intelligence (AI) security, and graph mining.



Lin Yuan received the B.Eng. degree in electronic science and technology from the University of Electronic Science and Technology of China (UESTC) in 2011 and the Ph.D. degree in electrical engineering from École Polytechnique Fédérale de Lausanne (EPFL), Switzerland in 2017. He is currently working as researcher at the School of Cyber Security and Information Law in Chongqing University of Posts and Telecommunications. His research interests include image and video analysis, multimedia privacy protection, and media forensics.



Nannan Wang received the B.Sc. degree in information and computation science from the Xi'an University of Posts and Telecommunications in 2009 and the Ph.D. degree in information and telecommunications engineering from Xidian University in 2015. He is currently a Professor with the State Key Laboratory of Integrated Services Networks, Xidian University, Xi'an, China. He has published over 150 articles in journals and proceedings including IEEE T-PAMI, IJCV, CVPR and ICCV. His research interests include computer vision and machine learning.



Kai Liang received the B.S. degree in electronic information engineering from the School of Electrical and Electronic Engineering, Chongqing University of Technology, Chongqing, China, in June 2021. He is currently pursuing the M.S. degree in electronic science and technology from the School of Photoelectric Engineering, Chongqing University of Posts and Telecommunications, Chongqing, China. His research interests include face privacy protection and face editing.



Xinbo Gao received the B.Eng., M.Sc., and Ph.D. degrees in signal and information processing from Xidian University, Xi'an, China, in 1994, 1997, and 1999, respectively. From 1997 to 1998, he was a Research Fellow with the Department of Computer Science, Shizuoka University, Shizuoka, Japan. From 2000 to 2001, he was a Post-Doctoral Research Fellow with the Department of Information Engineering, The Chinese University of Hong Kong, Hong Kong. Since 2001, he has been with the School of Electronic Engineering, Xidian University. He is



Xiao Pu received the Ph.D. degree in electrical engineering from École Polytechnique Fédérale de Lausanne (EPFL), Switzerland in 2018. She is currently working at the School of Cyber Security and Information Law in Chongqing University of Posts and Telecommunications. Her research interests include cross-modal semantic understanding and natural language processing.

currently a Cheung Kong Professor of Ministry of Education, a Professor of Pattern Recognition and Intelligent System, and the Director of the State Key Laboratory of Integrated Services Networks, Xi'an. His current research interests include multimedia analysis, computer vision, pattern recognition, machine learning, and wireless communications. He has published five books and around 200 technical articles in refereed journals and proceedings.